ELECTRONIC SUPPLEMENTARY INFORMATION FOR

Semiconducting Liquid Crystalline Dispersions with Precisely Adjustable Band Gaps and Polarized Photoluminescence

Tingting Zhou,[1,2] Penghao Guo,[1,2] Xuelian Jiang,[1,2] Hongbo Zhao,[1,2] Qing Zhang,[3] Pei-Xi Wang.[1,2]*

[1] School of Nano-Tech and Nano-Bionics, University of Science and Technology of China, 96 Jinzhai Road, Hefei, Anhui, 230026, P. R. China

[2] i-Lab, Suzhou Institute of Nano-Tech and Nano-Bionics of the Chinese Academy of Sciences, 398 Ruoshui Road, Suzhou Industrial Park, Suzhou, Jiangsu, 215123, P. R. China

[3] NANO-X Vacuum Interconnected Nanotech Workstation, Suzhou Institute of Nano-Tech and Nano-Bionics of the Chinese Academy of Sciences, 385 Ruoshui Road, Suzhou Industrial Park, Suzhou, Jiangsu, 215123, P. R. China

*Correspondence: pxwang2020@sinano.ac.cn

EXPERIMENTAL METHODS

Materials

Hydrochloric acid (37 wt.% in water, Sigma-Aldrich), hydrobromic acid (48 wt.% in water, Sigma-Aldrich), hydroiodic acid (57 wt.% in water, Sigma-Aldrich), manganese(II) acetate tetrahydrate (99%, Sigma-Aldrich), lead(II) oxide (99%, Sigma-Aldrich), n-butylamine (99.5%, Sigma-Aldrich), 2-phenylethylamine (99%, Sigma-Aldrich), phenylmethylamine (99%, Sigma-Aldrich), [(4-fluorophenyl)methyl]amine (97%, Sigma-Aldrich), [(4-chlorophenyl)methyl]amine (98%, Sigma-Aldrich), N,N-dimethylformamide (anhydrous, 99.8 %, Sigma-Aldrich), cis-9-octadecenoic acid (oleic acid; > 99.0 %, Sigma-Aldrich), cis-1-amino-9-octadecene (oleylamine; > 98.0 %, Sigma-Aldrich), chlorobenzene (anhydrous, 99.8 %, Sigma-Aldrich), and cyclohexane (anhydrous, 99.5 %, Sigma-Aldrich) were used as received.

Characterization

Photoluminescence emission spectroscopy was conducted on a Hitachi F-4600 Fluorescence Spectrophotometer and the perovskite liquid crystalline dispersions were sealed in quartz cuvettes with an optical path length of 1 mm. Field emission scanning electron spectroscopy was performed on a Hitachi Regulus 8230 Ultra-high Resolution Scanning Electron Microscope. Atomic force microscopy was conducted on a Bruker Dimension Icon Atomic Force Microscope with ScanAsyst. Samples for SEM and AFM observations were prepared by spin-coating the colloidal lyotropic liquid crystalline dispersions of perovskite nanoplatelets (about 100 mg per mL in chlorobenzene) onto flat silicon (111) surfaces at a spinning speed of 6000 revolutions per minute for 60 seconds followed by thermal annealing at 373 K for 10 minutes. Excess surfactants on the samples were removed by immersion in a large volume (50 mL) of cyclohexane for about 30 minutes then dried in a nitrogen or argon atmosphere. Powder X-ray diffraction patterns were collected on a Bruker D8 ADVANCE Diffractometer using copper K-alpha radiation (with a wavelength of 0.15406 nm). Polarized optical microscopy images were obtained from a BM2100POL Polarized Optical Microscope.

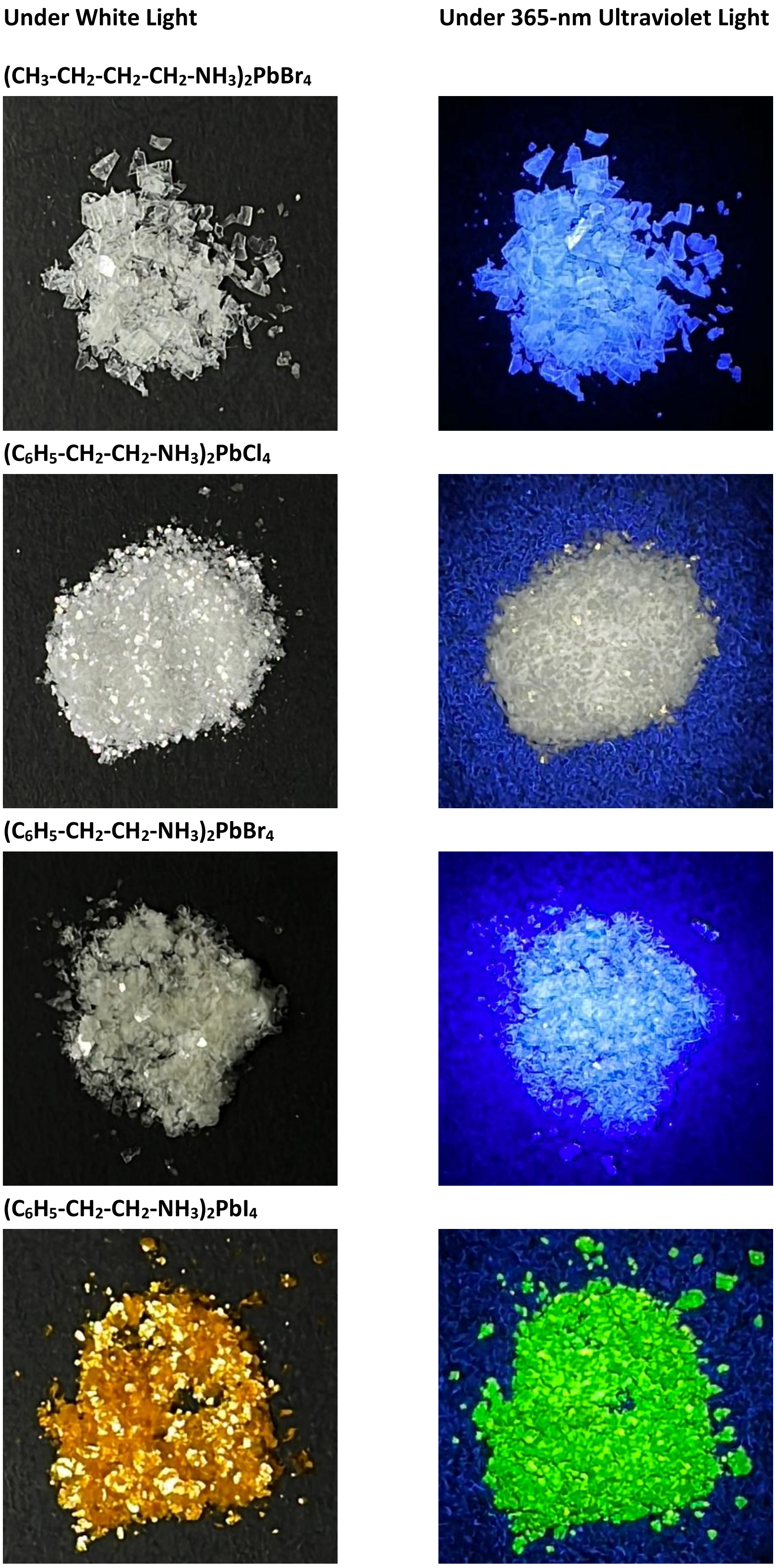

Figure S1. Photographs showing the synthesized two-dimensional organic-inorganic lead halide perovskite crystals of $(CH_3\text{-}CH_2\text{-}CH_2\text{-}CH_2\text{-}NH_3)_2PbBr_4$, $(C_6H_5\text{-}CH_2\text{-}CH_2\text{-}NH_3)_2PbCl_4$, $(C_6H_5\text{-}CH_2\text{-}CH_2\text{-}NH_3)_2PbBr_4$, and $(C_6H_5\text{-}CH_2\text{-}CH_2\text{-}NH_3)_2PbI_4$.

Under White Light **Under 365-nm Ultraviolet Light**

$(C_6H_5\text{-}CH_2\text{-}NH_3)_2MnCl_4$


$(4\text{-}F\text{-}C_6H_4\text{-}CH_2\text{-}NH_3)_2MnCl_4$


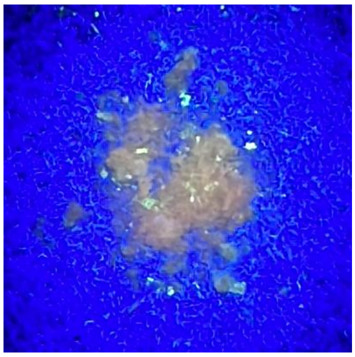

$(4\text{-}Cl\text{-}C_6H_4\text{-}CH_2\text{-}NH_3)_2MnCl_4$


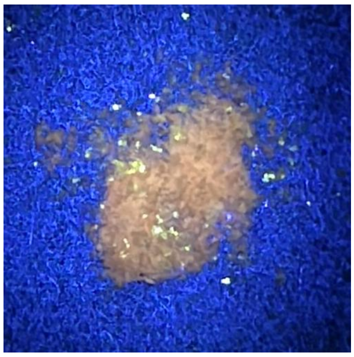

Figure S2. Photographs of the synthesized two-dimensional organic-inorganic manganese chloride perovskite crystals of $(C_6H_5\text{-}CH_2\text{-}NH_3)_2MnCl_4$, $(4\text{-}F\text{-}C_6H_4\text{-}CH_2\text{-}NH_3)_2MnCl_4$, and $(4\text{-}Cl\text{-}C_6H_4\text{-}CH_2\text{-}NH_3)_2MnCl_4$, where photos in the left column were taken under white light, while photos in the right column were taken under ultraviolet light with a wavelength of 365 nanometers.

$(C_6H_5\text{-}CH_2\text{-}NH_3)_2MnCl_4$

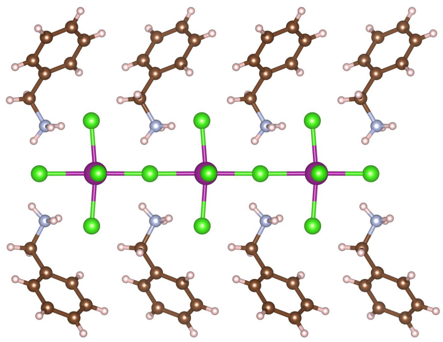

$(4\text{-}F\text{-}C_6H_4\text{-}CH_2\text{-}NH_3)_2MnCl_4$

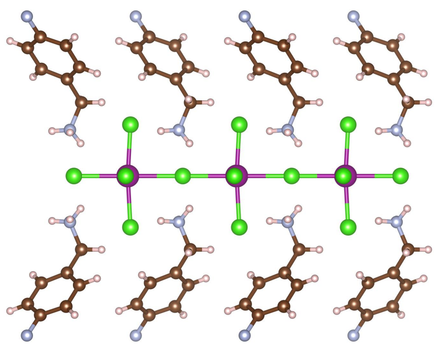

$(4\text{-}Cl\text{-}C_6H_4\text{-}CH_2\text{-}NH_3)_2MnCl_4$

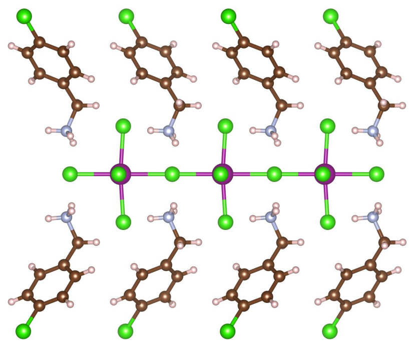

Figure S3. Crystal structures (obtained by single-crystal X-ray diffraction analysis) of perovskites $(C_6H_5\text{-}CH_2\text{-}NH_3)_2MnCl_4$, $(4\text{-}F\text{-}C_6H_4\text{-}CH_2\text{-}NH_3)_2MnCl_4$, and $(4\text{-}Cl\text{-}C_6H_4\text{-}CH_2\text{-}NH_3)_2MnCl_4$.

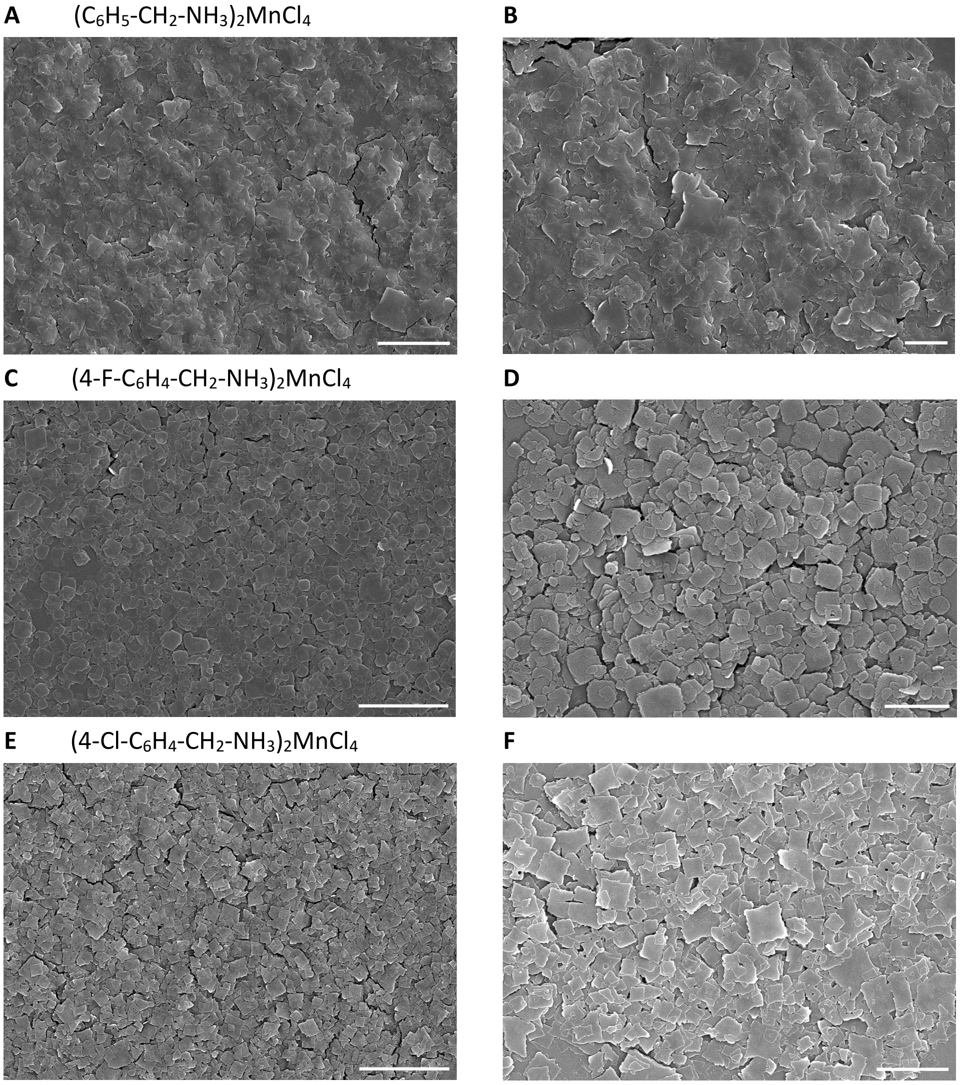

Figure S4. Scanning electron microscopy images showing plate-shaped colloidal nanocrystals of $(C_6H_5\text{-}CH_2\text{-}NH_3)_2MnCl_4$ (**A**,**B**), $(4\text{-}F\text{-}C_6H_4\text{-}CH_2\text{-}NH_3)_2MnCl_4$ (**C**,**D**), and $(4\text{-}Cl\text{-}C_6H_4\text{-}CH_2\text{-}NH_3)_2MnCl_4$ (**E**,**F**). Scale bars: 5 µm (**A**,**C**,**E**), 2 µm (**B**,**D**,**F**).

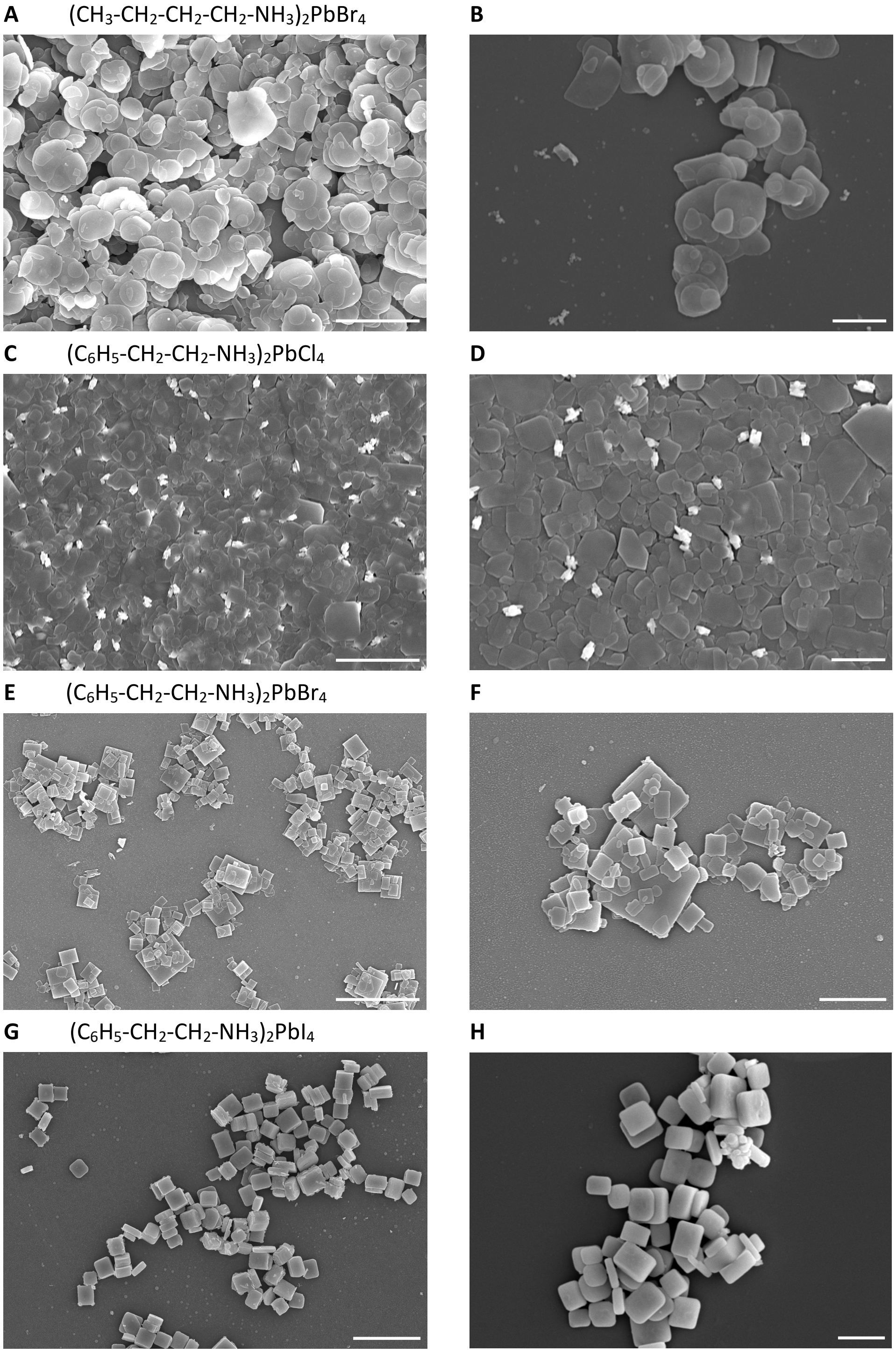

Figure S5. Scanning electron microscopy images of the colloidal nanoparticles of $(CH_3\text{-}CH_2\text{-}CH_2\text{-}CH_2\text{-}NH_3)_2PbBr_4$ (**A**,**B**), $(C_6H_5\text{-}CH_2\text{-}CH_2\text{-}NH_3)_2PbCl_4$ (**C**,**D**), $(C_6H_5\text{-}CH_2\text{-}CH_2\text{-}NH_3)_2PbBr_4$ (**E**,**F**), and $(C_6H_5\text{-}CH_2\text{-}CH_2\text{-}NH_3)_2PbI_4$ (**G**,**H**). Scale bars: 5 μm (**A**,**C**,**E**,**G**), 2 μm (**B**,**D**,**F**,**H**).

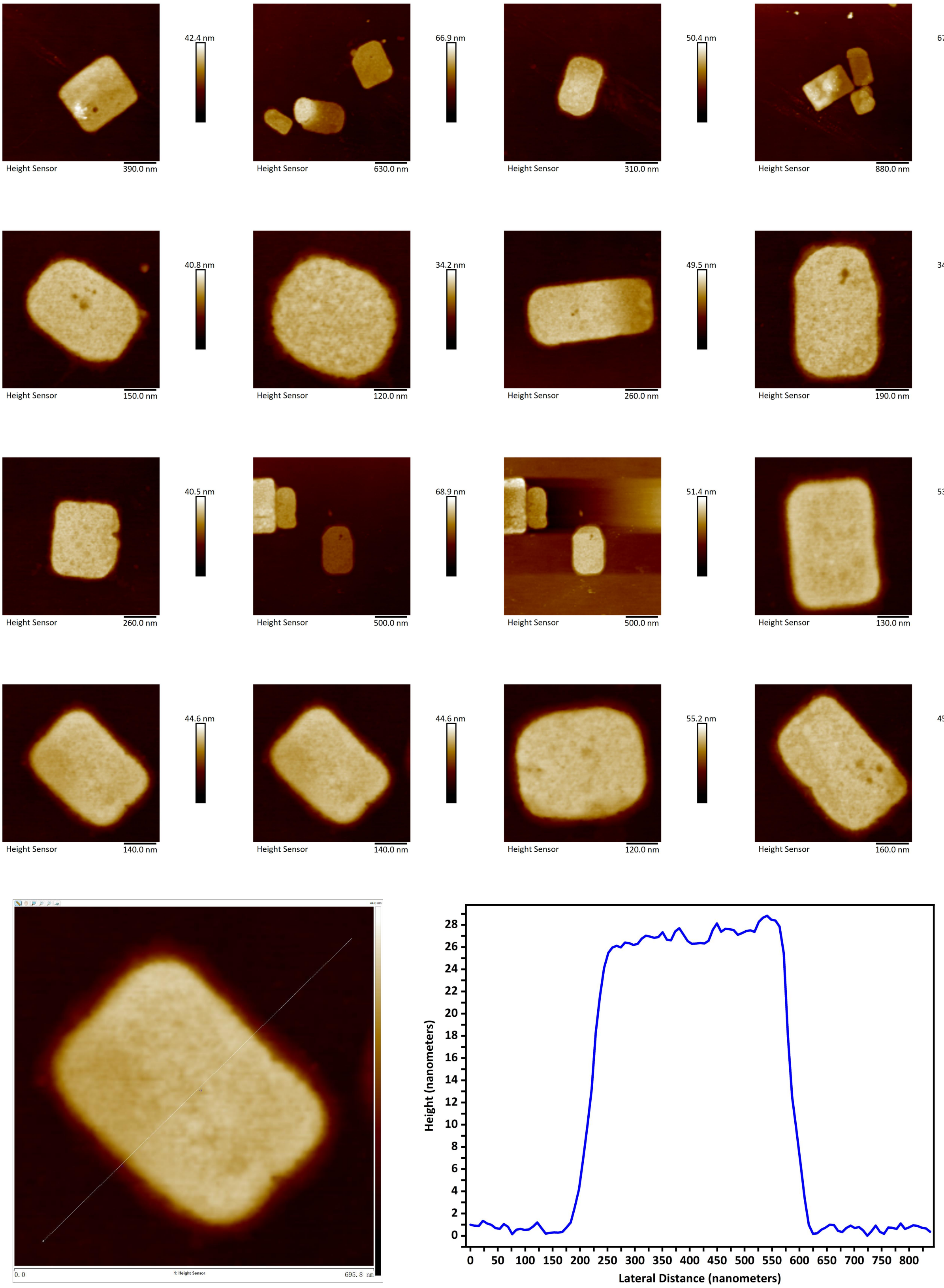

Figure S6. Atomic force microscopy images and height profiles showing lateral dimensions and thicknesses of different $(C_6H_5\text{-}CH_2\text{-}CH_2\text{-}NH_3)_2PbBr_4$ perovskite nanoplatelets.

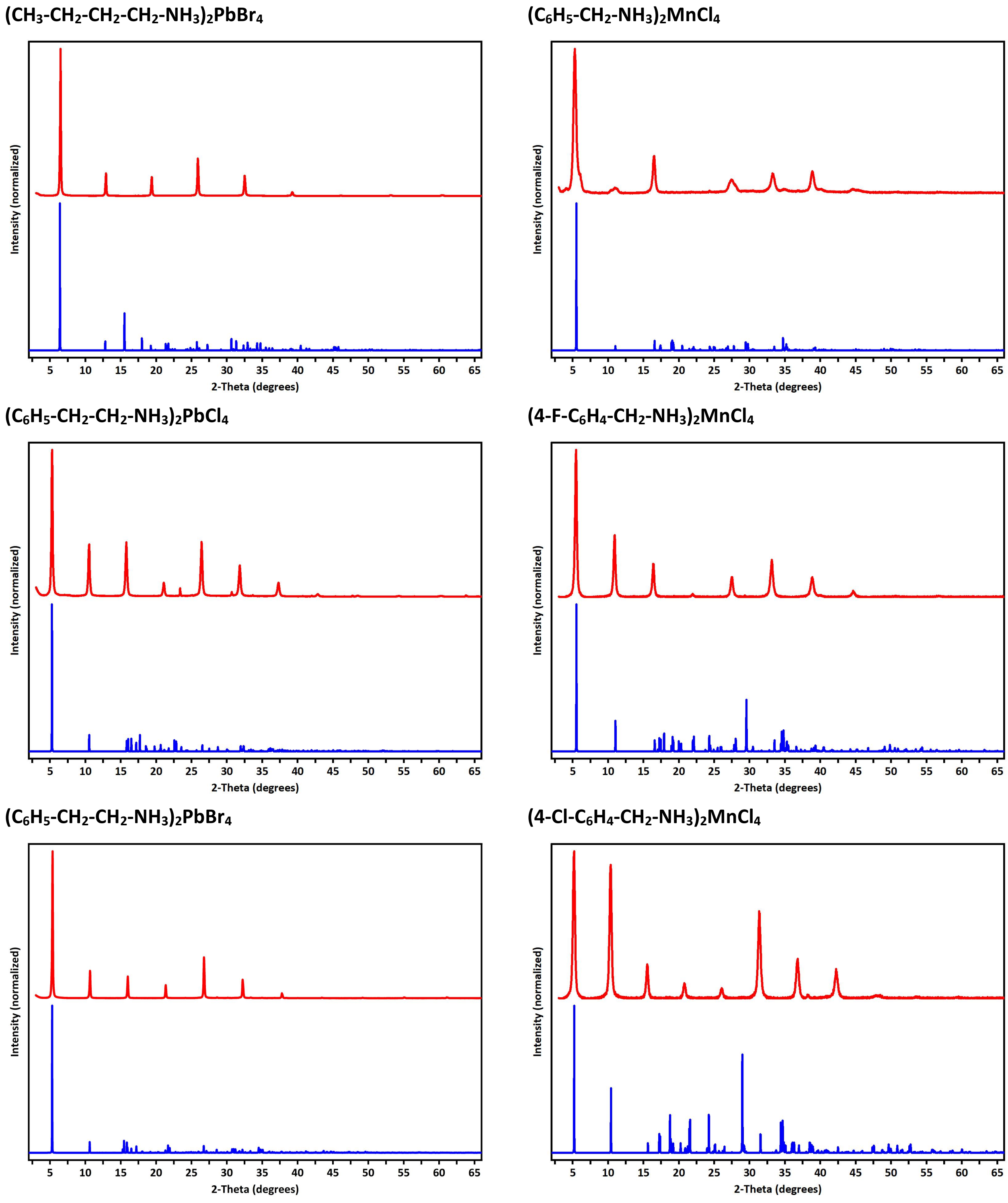

Figure S7. Powder X-ray diffraction patterns obtained by experimental measurements of spin-coated and dried thin films of colloidal liquid crystalline dispersions of perovskite nanoplatelets (upper red curves) and by simulations based on corresponding single-crystal X-ray diffraction data (lower blue curves).

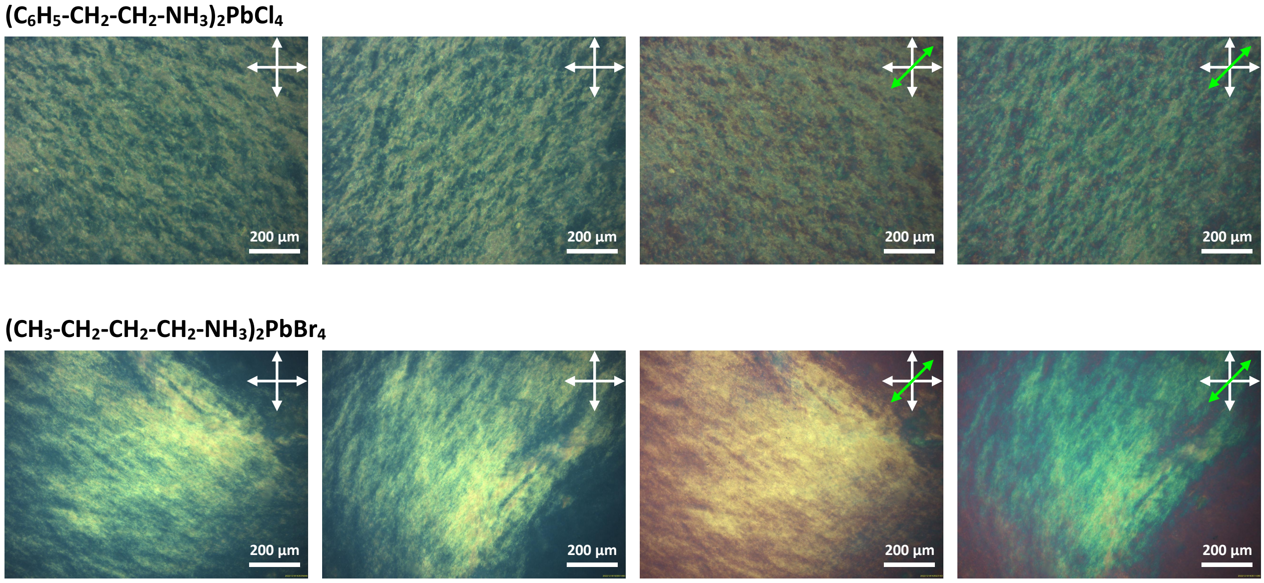

Figure S8. Polarized optical microscopy images showing the liquid crystalline phases formed by colloidal nanoplatelets of two-dimensional lead(II) halide perovskites. These samples were observed between two perpendicularly oriented linear polarizers (the left two columns) and with a 530-nm full-wavelength retardation plate (the right two columns).

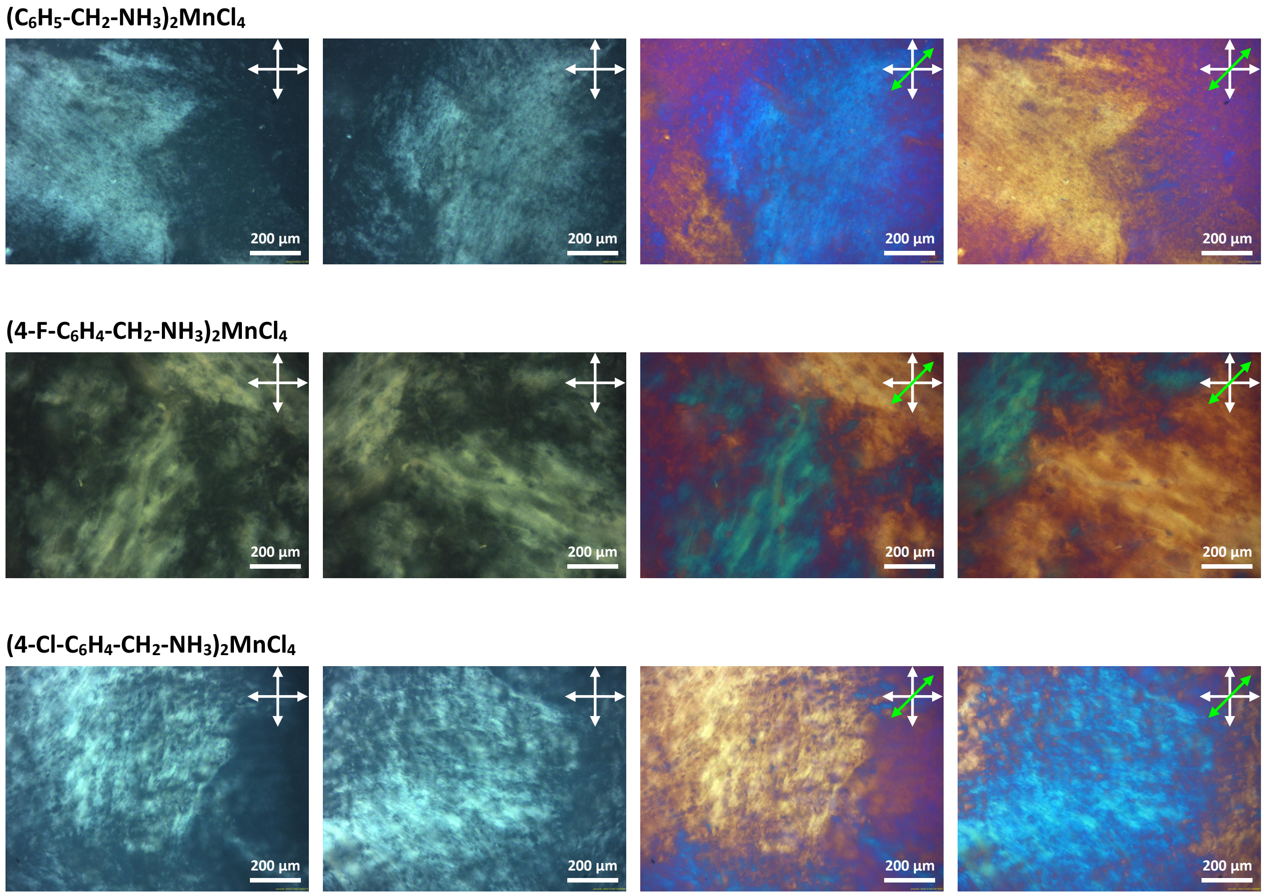

Figure S9. Polarized optical microscopy images showing the liquid crystalline phases formed by colloidal nanoplatelets of two-dimensional organic-inorganic manganese(II) chloride perovskites. In the left two columns, the samples were observed between two perpendicularly oriented linear polarizers; in the right two columns, a 530-nm full-wavelength retardation plate was inserted into the optical path.

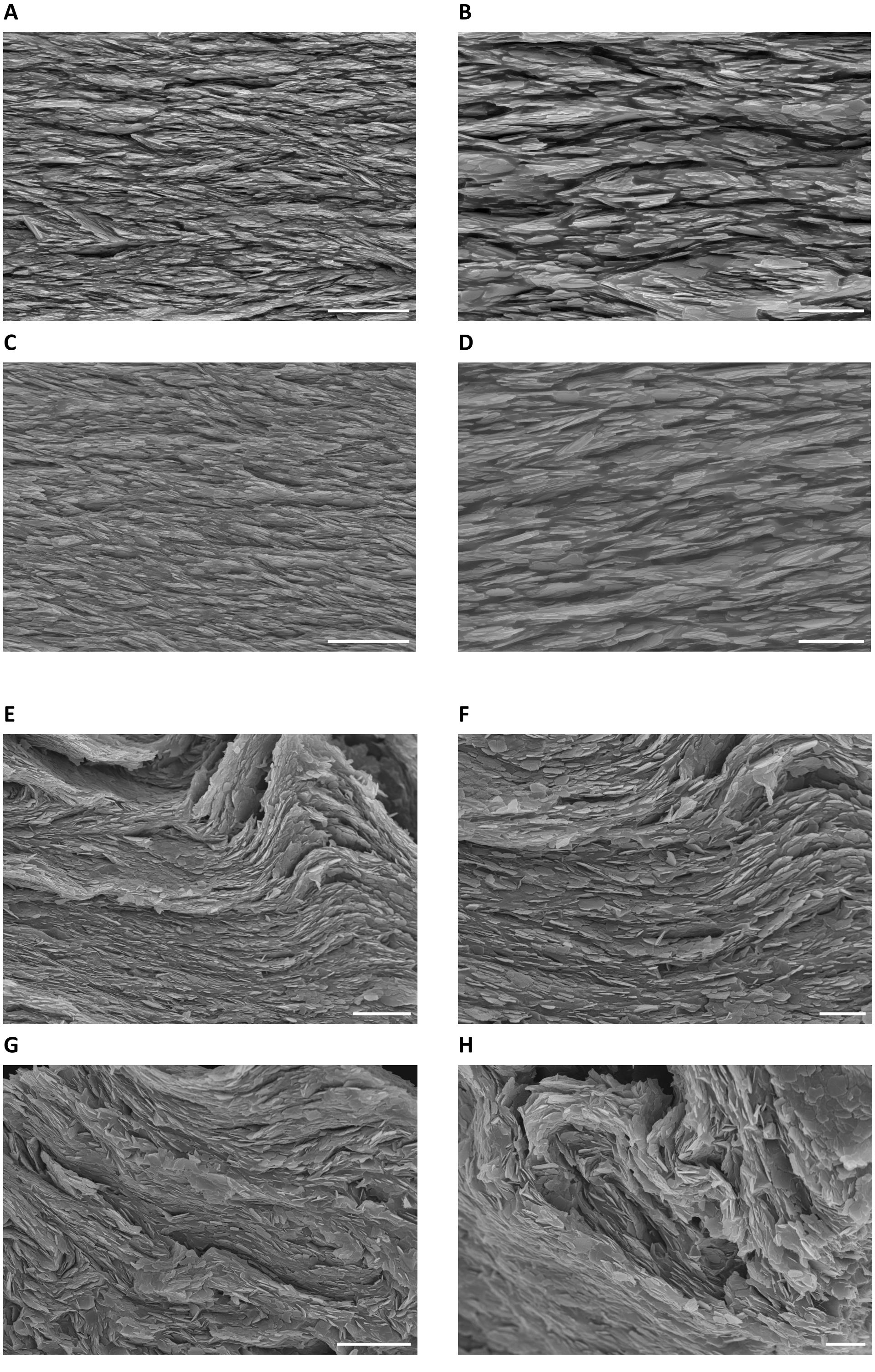

Figure S10. Cross-sectional scanning electron microscopy images showing the discotic nematic liquid crystalline phases formed by colloidal nanoplatelets of $(C_6H_5\text{-}CH_2\text{-}CH_2\text{-}NH_3)_2PbBr_4$ (**A-D**) and $(4\text{-}F\text{-}C_6H_4\text{-}CH_2\text{-}NH_3)_2MnCl_4$ (**E-H**). Scale bars: 5 µm (**A**,**C**,**E**,**G**), 2 µm (**B**,**D**,**F**,**H**).

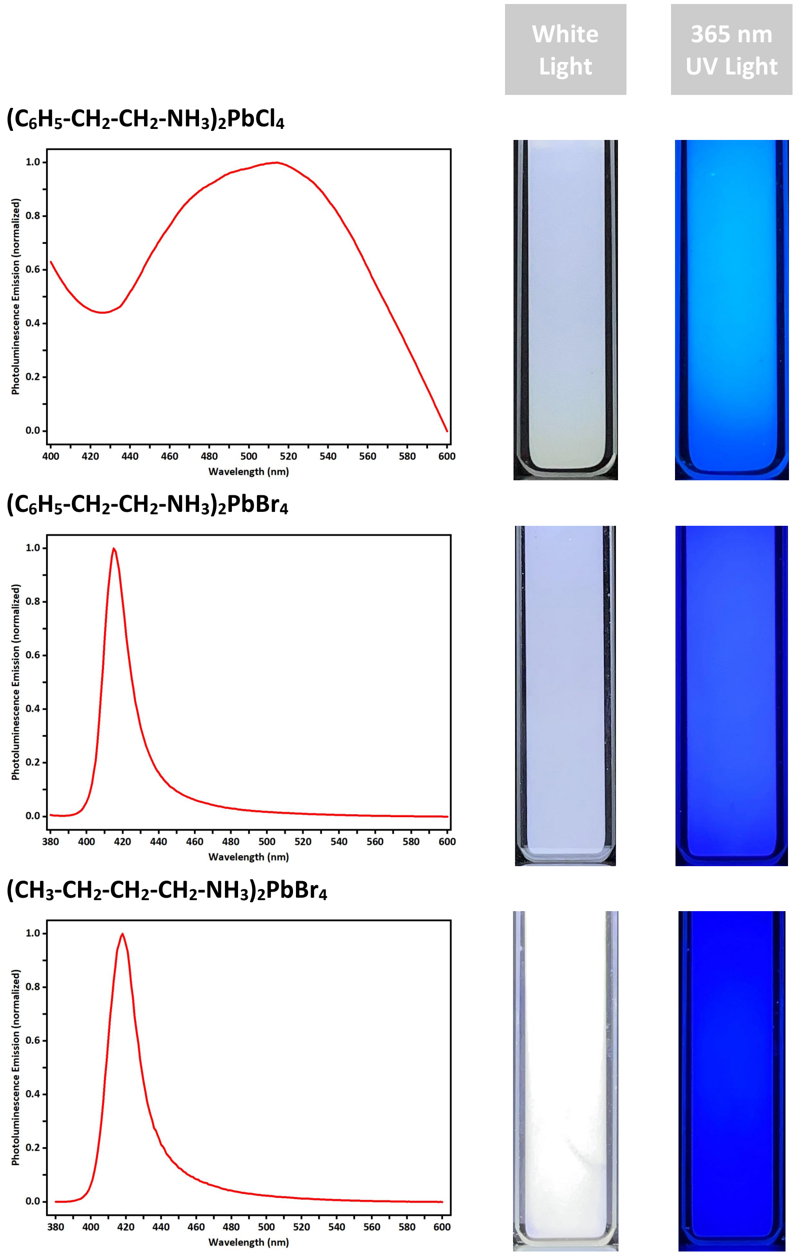

Figure S11. Photoluminescence emission spectra of the crystalline powders (red curves) and colloidal liquid crystalline dispersions (blue curves) of $(C_6H_5\text{-}CH_2\text{-}CH_2\text{-}NH_3)_2PbCl_4$, $(C_6H_5\text{-}CH_2\text{-}CH_2\text{-}NH_3)_2PbBr_4$, and $(CH_3\text{-}CH_2\text{-}CH_2\text{-}CH_2\text{-}NH_3)_2PbBr_4$. Photographs of these liquid crystals (sealed in quartz cuvettes with an internal width of 10 mm and an optical path length of 0.5 mm, observed under white light and 365-nm ultraviolet light) are displayed next to the spectra plots.

$(C_6H_5\text{-}CH_2\text{-}CH_2\text{-}NH_3)_2PbCl_2Br_2$

Photoluminescence Emission Spectrum

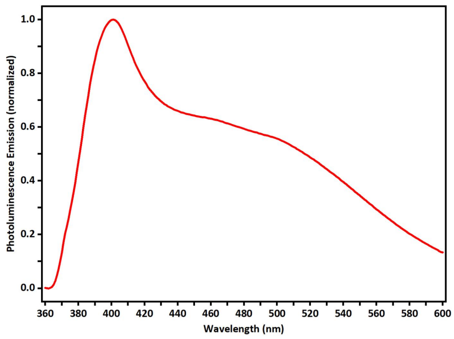

Powder X-ray Diffraction Patterns

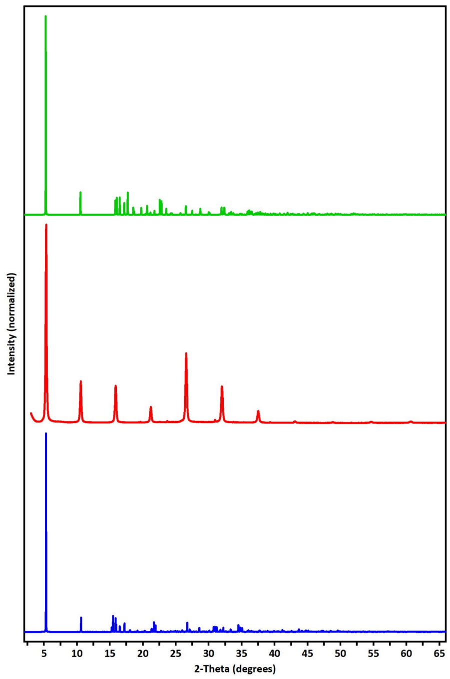

Figure S12. Additional data for liquid crystalline dispersions of $(C_6H_5\text{-}CH_2\text{-}CH_2\text{-}NH_3)_2PbCl_2Br_2$ perovskite nanocrystals:

(1) Photoluminescence emission spectrum.

(2) Photographs. The liquid crystal was sealed in a quartz cuvette with an internal width of 10 mm and an optical path length of 0.5 mm. The photos were taken under white light and 365-nm ultraviolet light.

(3) Powder X-ray diffraction pattern of a spin-coated and dried film of the liquid crystal (middle red curve). Simulated PXRD patterns (based on single-crystal X-ray diffraction profiles) of $(C_6H_5\text{-}CH_2\text{-}CH_2\text{-}NH_3)_2PbCl_4$ (upper green curve) and $(C_6H_5\text{-}CH_2\text{-}CH_2\text{-}NH_3)_2PbBr_4$ (lower blue curve) are also displayed for comparison.

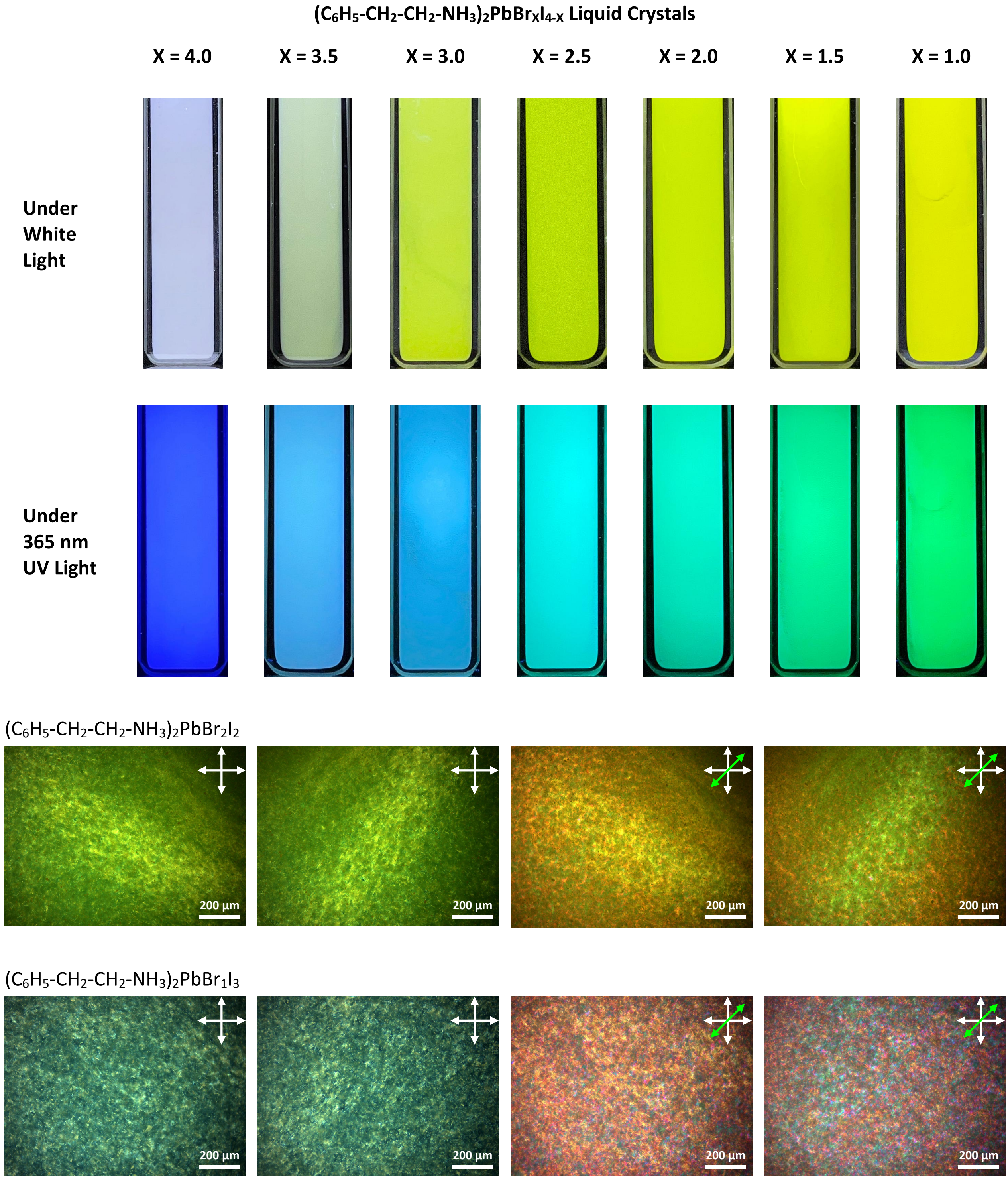

Figure S13. Additional data for $(C_6H_5\text{-}CH_2\text{-}CH_2\text{-}NH_3)_2PbBr_XI_{4\text{-}X}$ liquid crystals:

(1) Photographs. The liquid crystal was sealed in a quartz cuvette with an internal width of 10 mm and an optical path length of 0.5 mm. The photos were taken under white light and 365-nm ultraviolet light.

(2) Polarized optical microscopy images.

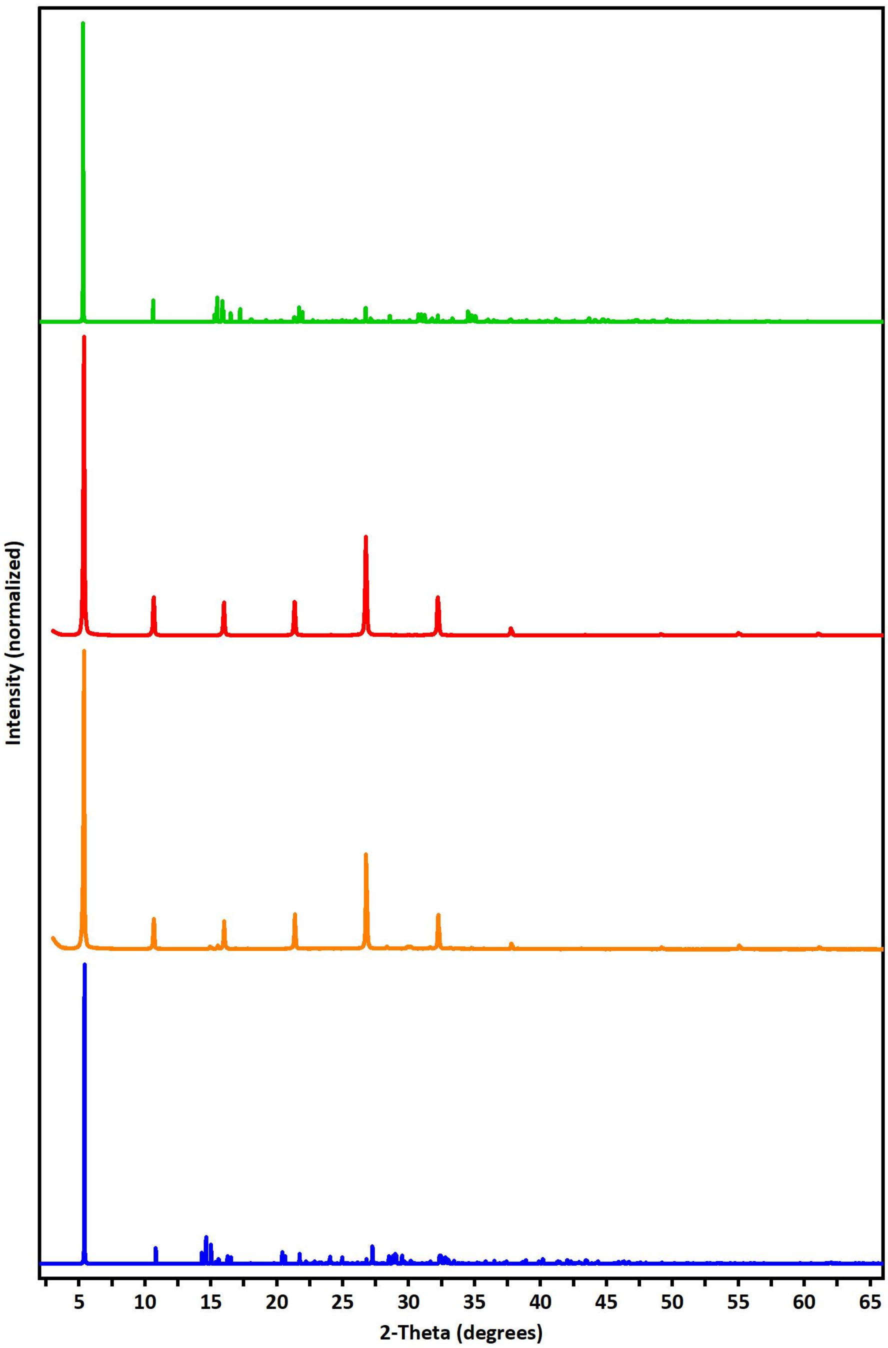

Figure S14. Powder X-ray diffraction patterns of spin-coated and dried films of colloidal liquid crystalline dispersions of $(C_6H_5\text{-}CH_2\text{-}CH_2\text{-}NH_3)_2PbBr_2I_2$ (red-colored curve) and $(C_6H_5\text{-}CH_2\text{-}CH_2\text{-}NH_3)_2PbBr_1I_3$ (orange-colored curve) perovskites. Simulated PXRD patterns (based on single-crystal X-ray diffraction profiles) of $(C_6H_5\text{-}CH_2\text{-}CH_2\text{-}NH_3)_2PbBr_4$ (green-colored curve at the top) and $(C_6H_5\text{-}CH_2\text{-}CH_2\text{-}NH_3)_2PbI_4$ (blue-colored curve at the bottom) are also displayed for comparison.

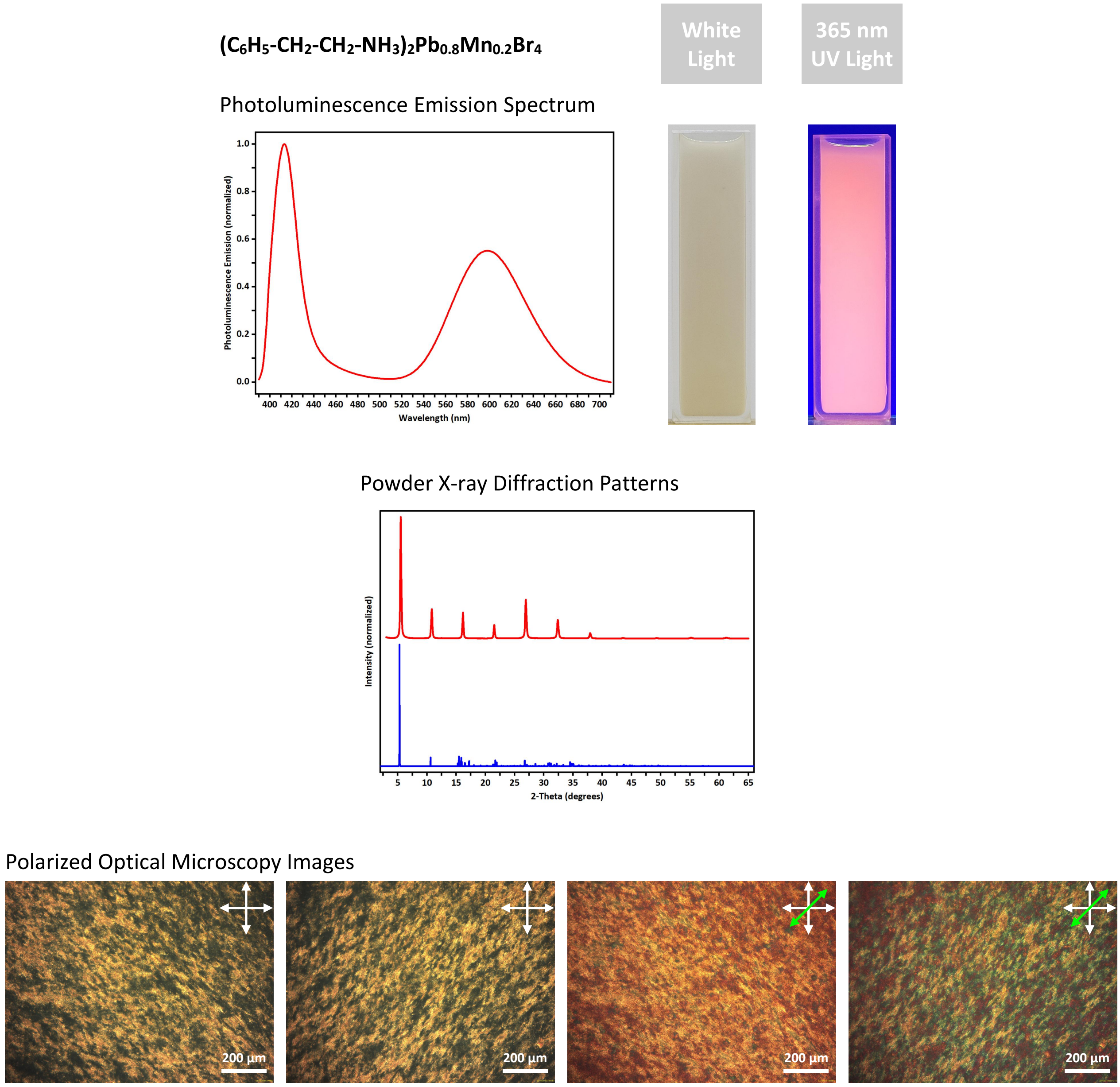

Figure S15. Additional data for (C_6H_5-CH_2-CH_2-NH_3)$_2$$Pb_{0.8}Mn_{0.2}Br_4$ perovskite liquid crystals:

(1) Photoluminescence emission spectrum.

(2) Photographs. The liquid crystal was sealed in a quartz cuvette with an internal width of 10 mm and an optical path length of 0.5 mm. The photos were taken under white light and 365-nm ultraviolet light.

(3) Powder X-ray diffraction pattern of a spin-coated and dried film of the liquid crystal (red curve). The simulated PXRD pattern (based on single-crystal XRD data) of (C_6H_5-CH_2-CH_2-NH_3)$_2$$PbBr_4$ (blue curve) is displayed for comparison.

(4) Polarized optical microscopy images.

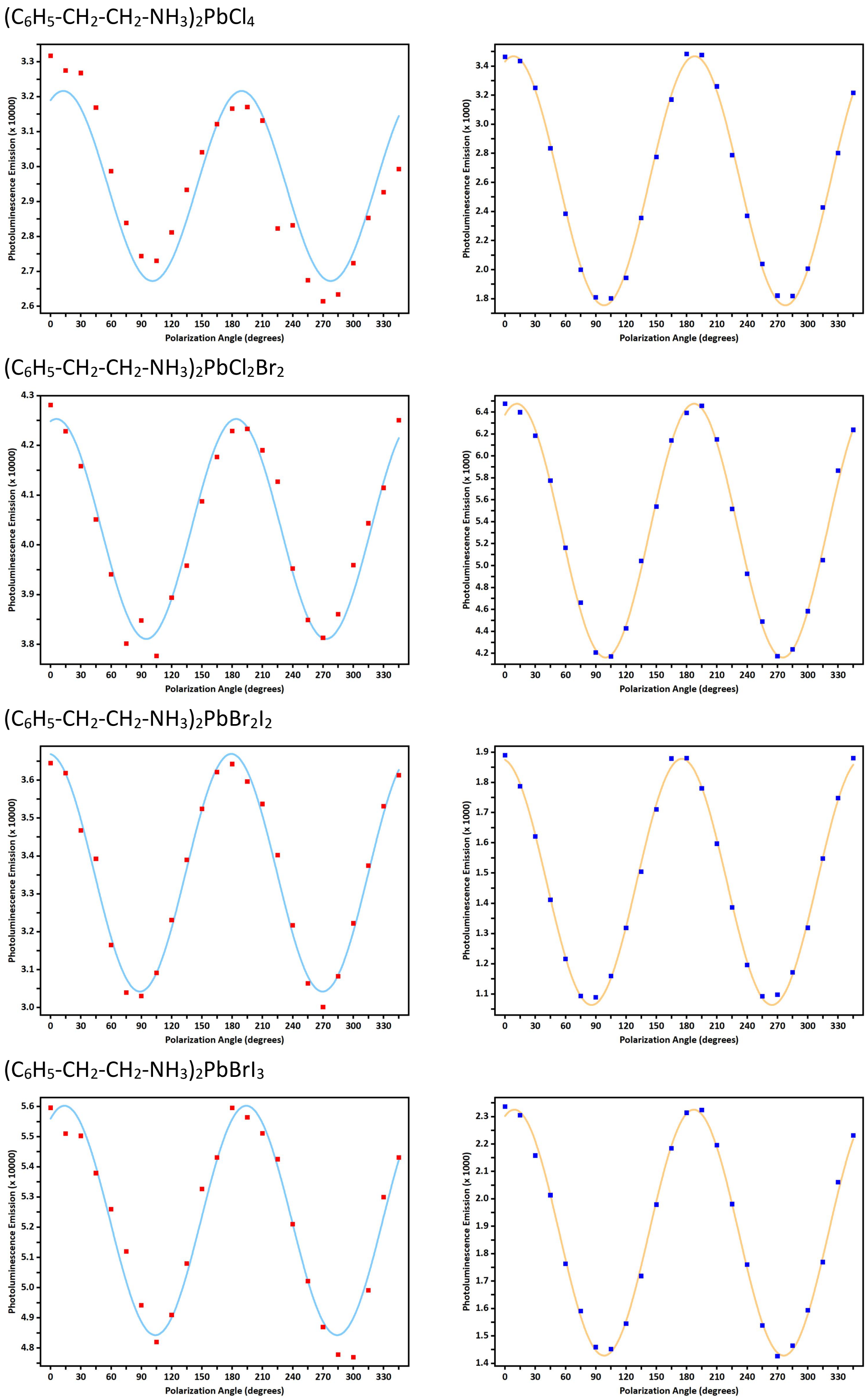

Figure S16. Linearly polarized photoluminescence (the left column) and polarization-dependent light-responsiveness (the right column) of colloidal liquid crystalline dispersions of $(C_6H_5\text{-}CH_2\text{-}CH_2\text{-}NH_3)_2PbCl_4$, $(C_6H_5\text{-}CH_2\text{-}CH_2\text{-}NH_3)_2PbCl_2Br_2$, $(C_6H_5\text{-}CH_2\text{-}CH_2\text{-}NH_3)_2PbBr_2I_2$, and $(C_6H_5\text{-}CH_2\text{-}CH_2\text{-}NH_3)_2PbBrI_3$ perovskite nanoplatelets (from top to bottom).

Table S1. Degree of polarization values of colloidal liquid crystalline dispersions of perovskite nanoplatelets.

	Polarized Photoluminescence Light Emission	Polarization-Dependent Light-Responsiveness
$(C_6H_5\text{-}CH_2\text{-}CH_2\text{-}NH_3)_2PbCl_4$	0.12	0.32
$(C_6H_5\text{-}CH_2\text{-}CH_2\text{-}NH_3)_2PbCl_2Br_2$	0.06	0.22
$(C_6H_5\text{-}CH_2\text{-}CH_2\text{-}NH_3)_2PbBr_2I_2$	0.10	0.27
$(C_6H_5\text{-}CH_2\text{-}CH_2\text{-}NH_3)_2PbBr_1I_3$	0.08	0.24